Proceedings of the Twenty-second (2012) International Offshore and Polar Engineering Conference **www.isope.org**
Rhodes, Greece, June 17–22, 2012

ISBN 978-1-880653-94–4 (Set); ISSN 1098-6189 (Set)

Near- and Far-field Tsunami Hazard from the Potential Flank Collapse of the Cumbre Vieja Volcano

Jeffrey C. Harris[1], *Stéphan T. Grilli*[1], *Stéphane Abadie*[2] *and Tayebeh Tajalli Bakhsh*[1]
1. Department of Ocean Engineering, University of Rhode Island, Narragansett, RI, USA
2. Laboratoire SIAME, Université de Pau et des Pays de l'Adour, Anglet, France

ABSTRACT

As demonstrated in the pioneering (but still controversial) work by Ward and Day (2001), the potential flank collapse of the Cumbre Vieja Volcano (CVV) on La Palma (Canary Islands) could result in a large tsunami having effects throughout the North Atlantic Ocean. While recent studies have suggested that such a collapse would likely result in more moderate tsunami waves than originally thought, these would still cause devastating effects in the near-field on neighboring Canary Islands, and their far-field coastal hazard would still be significant at some locations, and hence ought to be assessed. Abadie et al. (2011) simulated landslide tsunami generation from various CVV flank collapse scenarios, using a 3D Navier-Stokes (NS) multi-fluid VOF model (THETIS) with implicit slide motion. As 3D-NS computations are both too computationally demanding and affected by numerical diffusion, they computed near-field impact in a coupled long-wave Boussinesq model (FUNWAVE-TVD).

Here, for a similar series of CVV flank collapse scenarios (with 20, 40, 80, and 450 km^3 volume), we further simulate and analyze the near-field tsunami impact, and compute far-field propagation and coastal impact at distant locations (such as North America, western Europe and west Africa). A similar one-way model coupling approach is used between THETIS and a Cartesian, fully nonlinear version of FUNWAVE-TVD to compute near-field effects in a fine regional grid (about 15" arc mesh). Results in the latter grid are then used to initialize an ocean basin-scale grid (2' arc mesh) and compute far-field tsunami propagation, using a weakly nonlinear spherical coordinate version of FUNWAVE-TVD. Coastal impact is finally computed in selected locations using more finely resolved nested coastal grids (30" arc mesh). Results are analyzed in terms of wave/tsunami source characteristics, propagation features, and maximum wave elevation off distant coasts. For the most impacted coastal areas, further simulations will be performed in even finer nested grids, to compute inundation and runup. These results will be presented at the conference.

KEY WORDS: Tsunami; landslide; Navier-Stokes; VOF; Boussinesq wave models; volcano collapse; La Palma.

INTRODUCTION

Large landslides are inherent to the volcanic building process as material continuously accumulates until the point of slope failure (Holcomb and Searle, 1991). Debris avalanche deposits were for instance found in Hawaii (Moore et al., 1989; Robinson and Eakins, 2006) or at Réunion Island (Cochonat et al., 1990; Oehler et al., 2004). There is also clear geological evidence of past large paleo-submarine landslides of O(100 km^3) volume around the Canary Islands (Spain). Masson et al. (2002) identified at least 14 large landslides, which have occurred on the flanks of the youngest Canary Islands (i.e., El Hierro, La Palma, and Tenerife) in the last one million years, with the youngest one, at El Hierro, being only 15,000 years old. Even much smaller debris flows can be quite destructive: the tsunami triggered by the 0.5 km^3 Shimabara flank collapse in 1792 killed at least 4,000 people (Inoue, 2000), and two consecutive landslides of O(1 km^3) (first underwater and second subaerial) during the Stomboli eruption of 2002 produced local runup of 10 m (Tinti et al., 2005). Debris avalanches, orders of magnitude larger than these (i.e., up to hundreds of km^3), such as those identified in Hawaii or in the Canary Islands, have the potential for generating vastly more destructive waves (i.e., mega-tsunami; Ward and Day, 2001). Such potentially catastrophic events may occur in average every 100,000 years in the Canary Archipelago. However, low probability does not necessarily mean low risk; so for proper tsunami hazard assessment, the consequences associated with such catastrophic events must be carefully estimated and modeled.

Among all the volcanoes on the Canary Islands, Cumbre Vieja (CVV; see Figs. 1 and 2) is the fastest growing one (Carracedo et al., 1999), and hence may pose the largest threat of a flank collapse. In their pioneering (but still controversial) work, Ward and Day (2001) were the first to study tsunami generation and propagation from an extreme CVV western flank collapse scenario. In their simulations, they assumed a large volume of debris of about 500 km^3 and, using fairly simple models, predicted the generation of extremely large local waves, which decayed in the far-field to still large 10-20 m waves off of the US east coast. Both their catastrophic landslide scenario and wave model were questioned in later work (Mader, 2001; Pararas-Carayannis, 2002). More recently,

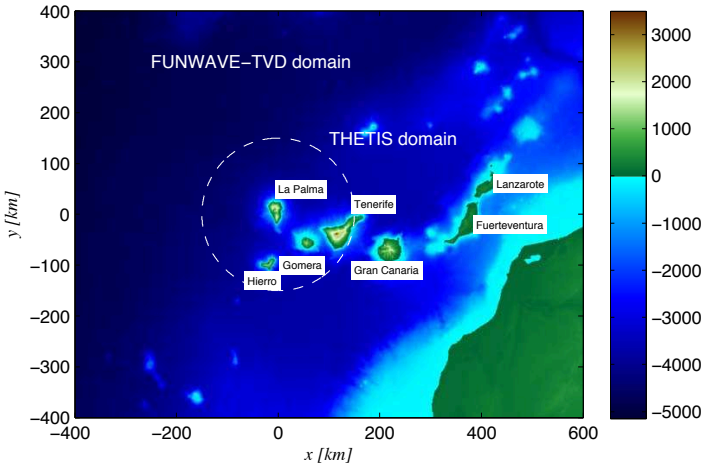

Fig. 1: Computational domains covering the Canary Islands, including the higher resolution 3D THETIS domain surrounding La Palma (dashed circle) and the 500 m resolution FUNWAVE-TVD domain (outer box).

some authors revisited this event and performed numerical simulations of both the same and other slide scenarios, using more accurate models of both landslide and wave generation/propagation (Pérignon, 2006; Grilli et al., 2006; Løvholt et al., 2008; Zhou et al., 2011). The likeliest rupture and CVV flank collapse scenario, however, are still subject of debate. This motivated Abadie et al. (2011) to develop slide scenarios based on slope stability analyses of the CVV western flank. Using these and more advanced models of landslide tsunami generation, Abadie et al. (2011) performed detailed near-field simulations (within the Canary Islands area), which predicted more moderate tsunami waves than originally proposed. Nevertheless, the resulting near-field impact on neighboring Canary islands and far-field coastal hazard might still be significant and hence ought to be assessed. This is the purpose of the present work detailed below.

LANDSLIDE TSUNAMI GENERATION

As in Abadie et al. (2011), the authors simulated landslide tsunami generation from various CVV flank collapse scenarios using the 3D Navier-Stokes (NS) multi-fluid VOF model THETIS. The latter model features, set up and application to the CVV landslide tsunami simulations are detailed below.

THETIS numerical model

THETIS is a three-dimensional (3D) general purpose multi-fluid NS solver, developed over the past 15 years by the TREFLE CNRS laboratory at the University of Bordeaux, France (http://thetis.enscbp.fr). In this model, the computational domain is assumed to be filled with one equivalent fluid, at all times, whose physical properties (namely density and viscosity) vary with space. Here, incompressible NS equations are solved with large-eddy simulations (LES), for water, air, and slide regions, represented as a single Newtonian fluid. [This, however, is not a limitation as non-Newtonian constitutive laws (i.e., Herschel-Bulkley generalized model) could be used.] In the present applications, turbulent dissipation is modeled using a mixed scale subgrid model (Lubin et al., 2006). The governing equations (i.e., conservation of mass and momentum) are discretized using the finite volume method, on a fixed staggered mesh, which may be Cartesian, cylindrical, or curvilinear. These governing equations are exact, except at interfacial grid cells, where momentum fluxes are only approximated, due to the presence of several fluids. All fluid-fluid interfaces are tracked using the VOF method (Hirt and Nichols, 1981). THETIS was used to model wave generation by deformable slides (Morichon and Abadie, 2010) and to simulate plunging breaking waves (Abadie et al., 1998; Lubin et al., 2006). Details of the model equations and implementation, as well as a thorough validation of THETIS for 2D and 3D rigid slide cases, can be found in Abadie et al. (2010).

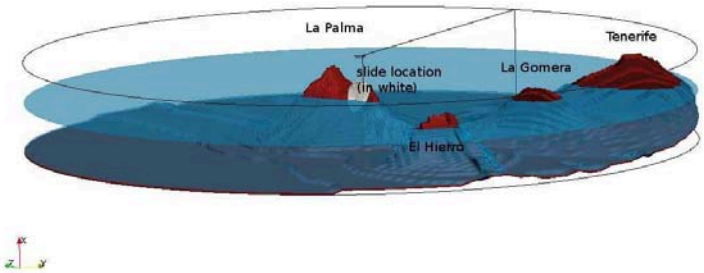

Fig. 2: Sketch of THETIS 3D computational domain for the simulation of landslide tsunami generation.

THETIS model setup

Figure 2 shows a sketch of THETIS' 3D computational domain, which is discretized with a cylindrical mesh (i.e., whose grid size grows with the distance away from the domain center), in accordance with the radial nature of wave propagation. The slide area is marked in white on the figure and corresponds to a 80 km^3 volume. Besides La Palma, the islands of El Hierro, La Gomera, and Tenerife have been included in the domain, since they affect the early stages of wave propagation. The computational domain is a 8 km tall cylinder with a 150 km radius; 300 grid cells are used in the radial direction (with a mesh stretched from 200 m in the initial slide area), 80 grid cells vertically (also stretched, with a minimum distance of 10 m), and 140 grid cells in the tangential direction (with a minimum spacing of 1.2° in the approximate direction of maximum tsunami energy (20° anticlockwise with respect to west). Bathymetry around La Palma was specified by digitizing maritime charts (Masson et al., 2002). Errors on horizontal distance in this digitalization were $\pm$500 m, to be compared to the 2 minute resolution (approx. 3,700 m) of ETOPO-2 data, e.g., used in Løvholt et al. (2008). With this grid, computations take one week in serial mode on a Mac Pro desktop computer (64 GB of RAM, two 2.93 GHz 6-core Intel Xeon processors) for 4 minutes of simulated time. For this reason, computations of sensitivity to slide volume and mesh parameters were performed on a large computer cluster, in parallel mode.

Based on slope stability analyses (Abadie et al., 2008; Fabre et al., 2011), four slide scenarios were considered in this study. The first two, with slide volumes of 40 and 80 km^3, were consistent with the stability analyses; a 20 km^3 was used as a lower case scenario and 450 km^3, as an extreme scenario, similar to those studied earlier (Ward and Day, 2001; Pérignon, 2006; Grilli et al., 2006; Gisler et al., 2006; Løvholt et al., 2008). Except for the 450 km^3 case, the slide initial geometry was obtained by taking the intersection between an ellipsoidal rupture surface and the digital terrain model. For the first 3 scenarios, the ellipsoid semi-major axis is directed North-South, with the two other axes inclined at 17° with respect to the horizontal and vertical directions, respectively, following the volcano slope. The slide center of mass is located 500 m above sea level, 2.5 km west, and 12 km north of La Palma's southern

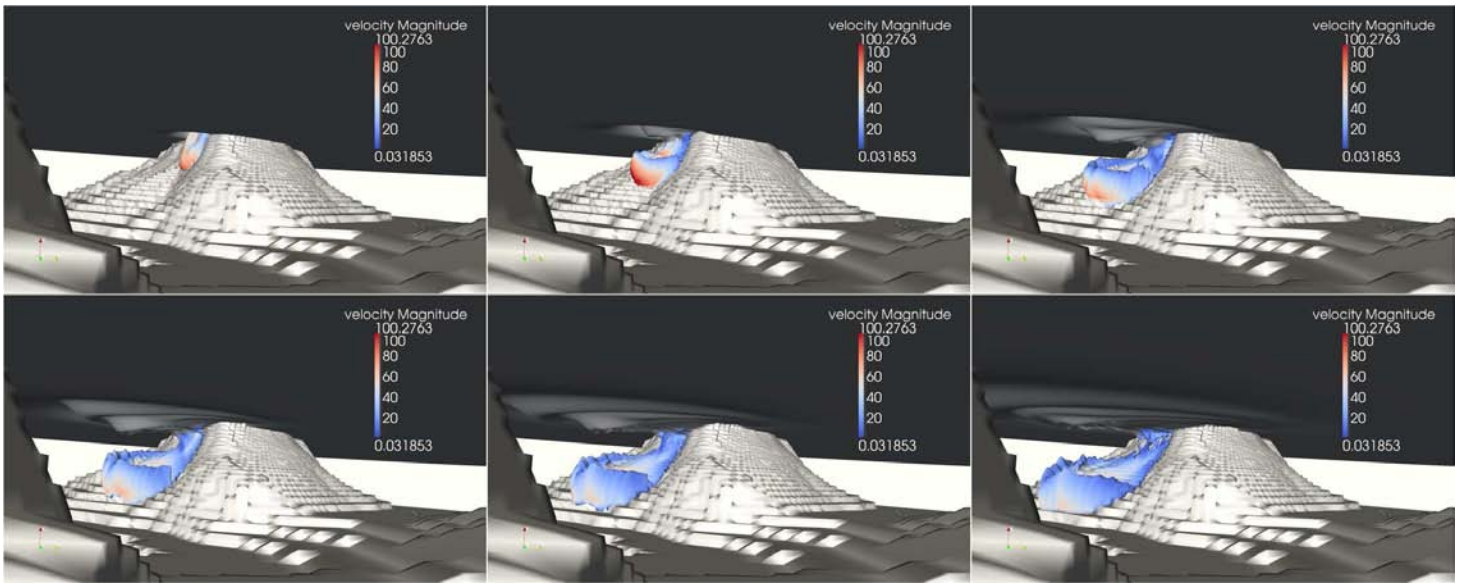

Fig. 3: Simulations of landslide tsunami generation with THETIS. Underwater views of water and slide interfaces (volume fractions respectively equal to 0.5 and 0.1) at t = a) 50 s, b) 100 s, c) 150 s, d) 200 s, e) 250 s, f) 300 s, for a slide initial volume of 80 km^3. Slide contour are colored by velocity magnitude.

cape. Finally, for the geometry of the 450 km^3 case, the same procedure as detailed in Løvholt et al. (2008) was followed. Note that the high safety factors found in the slope stability analyses indicate that the CVV western flank is rather stable under present conditions, although a large earthquake or volcanic eruption could trigger a slide.

In the present study (similar to Gisler et al., 2006), the authors modeled the CVV slide debris flow as an inviscid fluid, with a constant 2,500 kg/m^3 density (i.e., corresponding to basalt). As a result, basal friction is not modeled, nor resistance to internal deformation, which should yield more energetic and dynamic slides, likely to generate worst case scenario tsunamis. Results have been reported that support this assumption, indicating that large rock slides typically have large run-out distances, which are incompatible with large friction values (basal or internal) (e.g., Legros, 2002). Sensitivity analyses of tsunami generation to slide kinematics, and basal and internal friction are left out for future investigations.

Tsunami generation

Figure 3 shows results of THETIS simulations for the 80 km^3 CVV flank collapse scenario, consisting in six underwater snapshots for increasing time, displaying the air/water and water/slide interfaces. The 0.5 water volume fraction defines the air-water interface, while the 0.1 slide volume fraction defines the water/slide interface. [Note, the latter value was selected rather than 0.5 because, due to the combined effects of mixing and shearing, a 50% slide volume rate no longer occurs beyond some stage of slide motion.] The coupling between slide motion and free surface wave generation is quite clear on the figure, with a large depression wave being associated with the strong initial slide downward velocity, characteristic of large subaerial slides. For a long time, the slide then nearly travels at the speed of the leading generated surface wave, allowing for a large transfer of its energy to waves.

Figure 4 shows surface elevations computed at $t = 7.5$ min for all four scenarios. Tsunami directivity is similar in all cases (24° from west, except for the 20 km^3 scenario, where it is 18°), but maximum wave elevation increases and occurs farther away from the island, the larger the slide

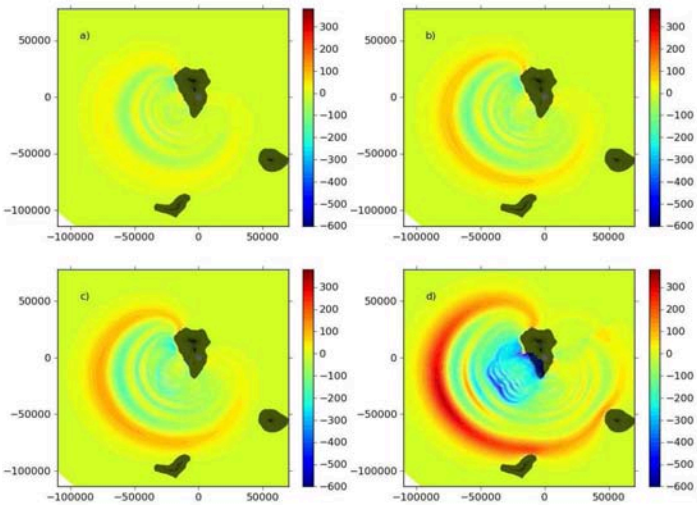

Fig. 4: THETIS 3D computations. Surface elevations (in meter; same scale) at $t = 7.5$ min, for slide volume: a) 20, b) 40, c) 80, d) 450 km^3.

volume. Hence, the leading wave average celerity slightly increases with slide volume, with (from results): 157 m/s for 20 and 40 km^3, 160 m/s for 80 km^3, and 173 m/s for 450 km^3; this is due to amplitude dispersion effects. By contrast, the distance between the first and second wave crests, which is a measure of wavelength, tends to decrease with slide volume, with (from results): 26.6, 24.4, 23.8 and 21.7 km, in each case respectively. The combination of larger height and shorter wavelength yields increasingly steeper, and thus nonlinear leading waves, as slide volume increases. In the latter case, shown in Fig. 4d, for instance, the leading wave characteristics are: $H/L = 0.032$; $kH = 0.20$; $kh = 0.87$ (for depth $h = 3000$ m), while the limiting steepness is about $(H/L)^{max} = 0.098$; hence, the leading wave steepness is about one-third the maximum steepness. Furthermore, $kh > \pi/10 = 0.314$, the standard limit for long waves, indicating this is an intermediate water wave, for which frequency disper-

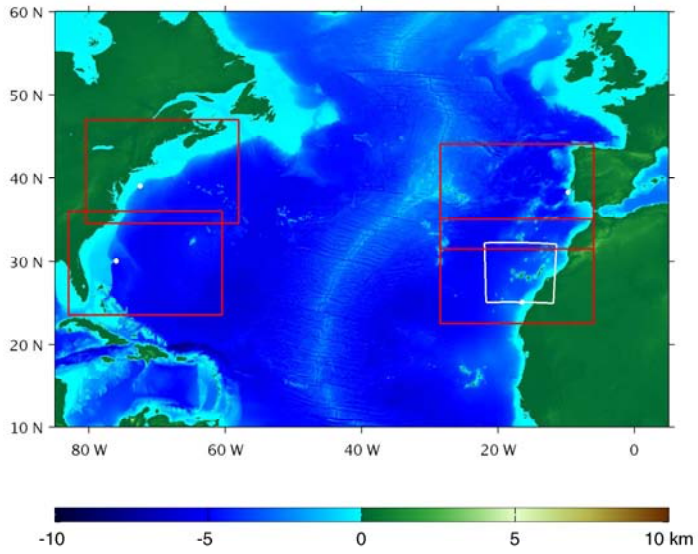

Fig. 5: FUNWAVE-TVD far-field simulation grids: 500 m regional Cartesian grid (white box); 2' arc spherical Atlantic grid (outer box); 30" Cartesian grids for simulating far-field coastal effects (red boxes). White dots mark the locations of four stations (off New York, Florida, Lisbon, and the Sahara) where time-series were recorded in 2' grid).

	Latitude	Longitude	Resolution
Atlantic	10.0° N–60.0° N	85.0° W–5.0° E	2'
N. North Am.	34.5° N–47.0° N	80.5° W–58.0° W	30"
S. North Am.	23.5° N–36.0° N	83.0° W–60.5° W	30"
Europe	31.5° N–44.0° N	28.5° W–6.0° W	30"
Africa	22.5° N–35.0° N	28.5° W–6.0° W	30"

Table 1: Data for FUNWAVE-TVD simulation grids of Fig. 5.

sion effects are important. Other waves in the tsunami train, which are even shorter, have larger kh values and hence feature increasingly large dispersive effects.

NEAR- AND FAR-FIELD TSUNAMI IMPACT

FUNWAVE-TVD numerical model

As discussed before, it would be too computationally costly to use the 3D model THETIS beyond the region directly surrounding La Palma, for simulating tsunami impact from the CVV flank collapse both in the near-field, on neighboring Canary islands, and beyond in the far field. Instead, a coupled approach is used, in which near- and far-field simulations are performed with the (2D-horizontal) Boussinesq Model (BM) FUNWAVE-TVD, initialized with the 3D THETIS model results. FUNWAVE-TVD is a recent improvement of the FUNWAVE model (Wei et al., 1995; Kennedy et al., 2000; Chen et al., 2000, 2003; Kirby, 2003), which was originally designed and used for simulating coastal and nearshore waves, but was later successfully applied to a variety of tsunami case studies, both landslide and co-seismic (e.g., Watts et al., 2003; Days et al., 2005; Grilli et al., 2007; Ioualalen et al., 2007; Tappin et al., 2008; Karlsson et al., 2009; Grilli et al., 2010). FUNWAVE-TVD was developed as a fully nonlinear version in Cartesian coordinates (Shi et al., 2012), but currently only as a weakly nonlinear approximation in spherical coordinates with Coriolis effects (Kirby et al., 2009, 2012). The former model will be used for the simulations in the near-field coastal grids, while the latter will be used in the far-field simulations in the Atlantic Ocean basin scale grid (Fig. 5).

As they include frequency dispersion effects, BMs simulate more complete physics than models based on Nonlinear Shallow Water Equations (NSWE), which until recently have traditionally been used to model co-seismic tsunami propagation. This is particularly important for simulating landslide tsunami propagation, for which waves as shown above in THETIS results for the CVV case, are shorter and hence more dispersive than for co-seismic tsunamis. FUNWAVE-TVD is based on the equations of Chen (2006) and Shi et al. (2012), which use a combined finite-volume and finite-difference MUSCL-TVD scheme. As in FUNWAVE (Wei et al., 1995), improved linear dispersive properties are achieved, up to the deep water limit, by expressing the BM equations in terms of the horizontal velocity vector at 0.531 times the local depth. Additionally, wave breaking is more accurately modeled by switching from the Boussinesq equations to the NSWE, when the local height to depth ratio exceeds 0.65. FUNWAVE-TVD's latest implementation is fully parallelized using MPI, for efficient use on distributed memory clusters. This model was fully validated using all of NOAA's National Tsunami Mitigation Program (NTHMP) mandatory benchmarks (Tehranirad et al., 2011).

In order to estimate inundation and runup on La Palma and other islands, a high resolution 500 m regional grid is used in near-field CVV simulations (Fig. 1). [Note, accurate runup simulations would require using even finer local grids around the most impacted areas.] In the modeling of outgoing waves, this grid allows resolving the shorter trailing waves generated by the CVV slide (Fig. 4). As depth rapidly drops to around 4.5 km offshore of the island, these trailing waves become increasingly dispersive (with $kh > \pi$), which justifies using an extended BM in the simulations. The Global Multi-Resolution Topography (GMRT) database (Ryan et al., 2009) is used to specify the bathymetry in this regional grid. While THETIS used the same high-resolution bathymetry near La Palma, because of the different grid interpolation schemes, there are slight differences in the bathymetry used by the two models. This however has negligible effects on results, as will be detailed below in the validation of the initialization process. As indicated before, the fully nonlinear Cartesian coordinate implementation of FUNWAVE-TVD is used in the regional grid, which allows accurately computing nonlinear effects in nearshore waves. A transverse secant Mercator projection is used in the latter grid, to correct for earth's sphericity (similar to the UTM system), with its origin at 28.5° N and 18.5° W (corresponding to -69 km, -14 km). This transformation leads to some small grid distortions, which are however deemed negligible. [After the coordinate transformation the largest distance between adjacent cells is 502.1 m, and the smallest distance is 496.4 m, giving a distortion of less than one percent, which is deemed acceptable.]

As mentioned, the tsunami transoceanic propagation is computed with the spherical version of FUNWAVE-TVD. Figure 5 shows the extent of the 2' arc grid used to this effect; the bathymetry is specified in this grid from the ETOPO1 database (i.e., 1' arc accurate). This simulation is initialized using results from the 500 m regional grid (also shown on the figure). Finally, far-field coastal effects are computed in 30" nested grids (Fig. 5), also using bathymetry from ETOPO1. Table 1 gives more specific information of the extent of the simulation grids.

Validation of THETIS-FUNWAVE model coupling

The coupling of THETIS with FUNWAVE is performed by using the 3D-VOF-NS solution at $t = 300$ s as an initial condition for FUNWAVE, be-

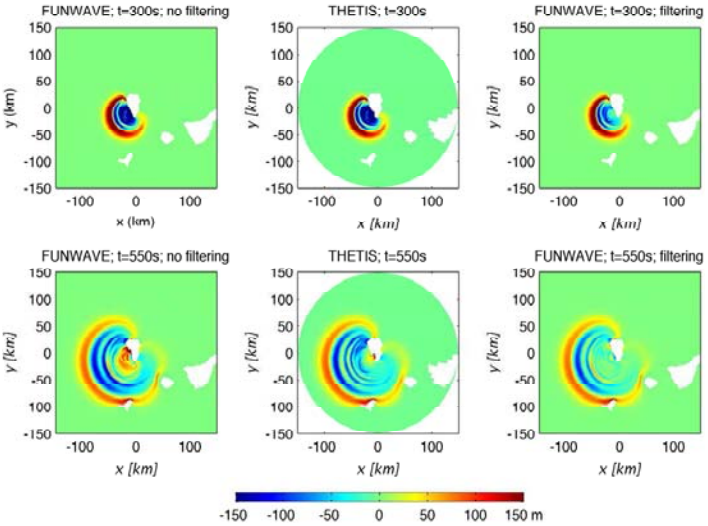

Fig. 6: Test of model coupling for the 80 km^3 case, when modeling wave propagation from $t = 300$ to 550 s using : (i) FUNWAVE without filtering of the initial conditions; (ii) THETIS; and (iii) FUNWAVE with filtering of the initial conditions.

fore the leading edge of the tsunami has reached the edge of the THETIS domain; i.e., this is a one-way coupling. Although at this time the slide has not yet come to a stop and there is still turbulent flow in the 3D domain, results show that all of the energy transfer from slide to waves has already occurred (Abadie et al., 2011). The NS velocity field is depth-averaged and the averaged horizontal velocity, together with the free surface elevation are interpolated onto the FUNWAVE mesh. This results in a slight error (2nd-order in kh), as the BM equations are framed in terms of a single horizontal velocity at a reference depth, but this has little effect on the results and has the advantage of averaging out the turbulent flow in the vertical direction. As seen in THETIS' 3D results, the tsunami wave train generated by the CVV slide, after a series of 3-4 larger and longer, long-crested, leading waves, features very short and irregular trailing waves, which result from the 3D highly turbulent residual flow induced by the slide near its initial location in La Palma. This turbulent flow is initially associated with short waves, but vertical mixing, which is most active around the slide tip, dissipates this flow without transferring energy to the outgoing leading waves. As this flow is not responsible for any significant tsunami coastal impact on La Palma, more distant islands, or in the far-field, and cannot be accurately represented in the BM, it seems reasonable to filter the NS solution prior to using it for initializing FUNWAVE (as further described in Abadie et al., 2011). An ad hoc filtering method (Fig. 6) was determined through numerical experimentation, which consisted in multiplying the output of THETIS (i.e., free-surface elevation and each velocity component) by a spatially varying function, removing the interior flow while keeping a smooth initial condition for FUNWAVE. This function is Gaussian, with a standard deviation of 15 km and the origin located at coordinates (-10 km, -10 km).

Prior to performing longer-term propagation simulations in FUNWAVE, the authors verified that this coupling approach provided reasonable initial results, for at least the first few leading waves, since most of the near-field run-up and inundation will be caused by these waves, and, in the far-field, by waves originated from these waves through frequency dispersion. This was done by initializing FUNWAVE using THETIS results at $t = 300$ s and performing simulations with both models for

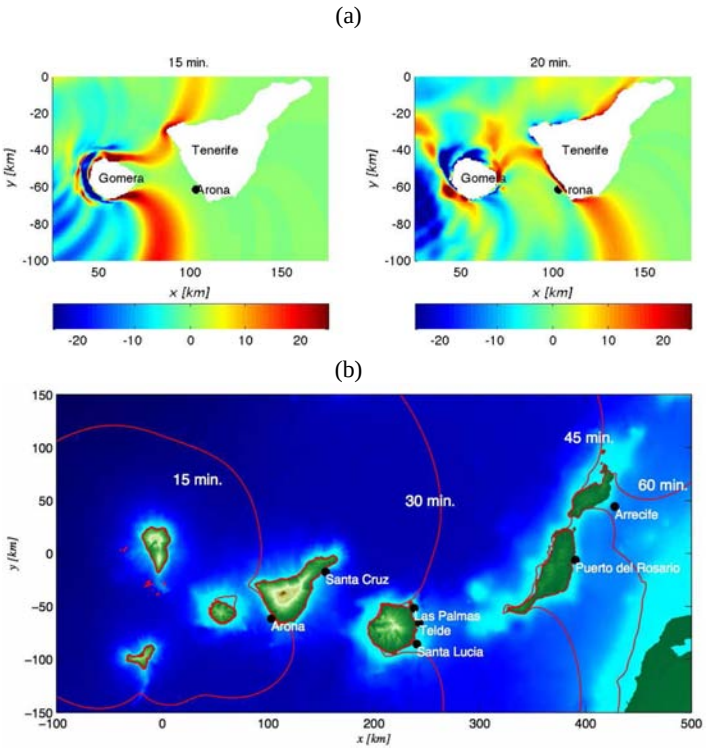

Fig. 7: FUNWAVE simulations in 500 m regional grid, for 80 km^3 CVV scenario, of near-field impact on neighboring islands: (a) wave field, 15 and 20 min. after the landslide; (b) travel time to various Canary Islands.

an additional 250 s. To assess the effects of filtering THETIS results, FUNWAVE computations were performed using both unfiltered and filtered results. Free surface elevations computed in both models were then compared at $t = 550$ s. Fig. 6 shows results for the 80 km^3 case. Although FUNWAVE's unfiltered results appear reasonable as compared to THETIS', as expected, there is not enough near-shore dissipation of shorter waves, which stay in the back of the FUNWAVE train, but do not persist in THETIS results. Besides causing unrealistically large short waves to appear near La Palma, using unfiltered results also affects at least the 3rd leading wave in the tsunami train. This is greatly improved in FUNWAVE's filtered results, which compare well to THETIS'; both the large short waves near La Palma dissipate and the 3rd leading wave now agrees well with THETIS results. While results are only shown for the 80 km^3 slide, it was verified that the overall quality of the comparison is similar for all four scenarios.

Near-field impact

Fig. 4 shows waves generated around La Palma at $t = 300$ s, based on results of 3D THETIS simulations. Results indicate that, while waves propagating faster than the slide are no longer influenced by its motion, the mean water level above and behind the slide is significantly lowered, resulting in a strong run-down at the coast (of more than 300 m at $t = 232$ s for the 80 km^3 case). Because of this phenomenon caused by mass conservation, the free surface elevation behind the leading wave is globally negative and remains so even after a long time of propagation. This is clear, for instance, in THETIS results for the 80 km^3 case at $t = 550$ s (Fig. 6). At this time, the tsunami wave train starts impacting the islands of Hiero and Gomera and is composed of an elevation wave, more than

100 m high, followed by an oscillatory train of lower amplitude waves, whose crests only raise up to near the still water level ($z = 0$). At the same time, the same figure shows that two elevation edge waves are propagating around La Palma on both sides of the island. Detailed results would show that these waves meet in the back of the islands near the populated city of Santa Cruz, which lies just above sea level, causing a 100 m runup at around $t = 700$ s. As indicated above, another important phenomenon on La Palma is a large free surface depression occurring near the initial location of the slide; this is followed by a violent backwash. Results would show that, at $t = 474$ s, the (return) fluid flow enters the cavity initially filled by the slide, generating a large runup, with a maximum value of 290 m on the northern part of the cavity.

While Fig. 4 shows that the majority of wave generation and propagation occurs in a general westward direction, there is also a significant eastward propagation of sizable waves, which can severely impact neighboring islands, owing to their proximity (as seen for Hiero and Gomera). This is clearer in Fig. 7a, which shows results of FUNWAVE simulations in the 500 m regional grid; for the same 80 km^3 case, large waves are impacting Gomera and Tenerife 15-20 min. after the slide, causing 10-24 m runup in the latter island. Fig. 7b shows that other islands would be impacted at later times; after waves pass by Gran Canaria (30 min.), causing 5-9 m runup, they propagate towards the easternmost islands, impacting the length of Fuerteventura and Lanzarote almost simultaneously (45 min.) and causing a moderate runup, up to 2 m, likely due to protection offered by the other islands.

	New York	Florida	Portugal	Sahara
Latitude	39.0°N	30.0°N	38.25°N	25.0°N
Longitude	72.5°W	76.0°W	9.75°W	16.5°W
Depth	1.6 km	5.0 km	2.0 km	0.9 km
Arrival time	6.6 hr.	6.9 hr.	1.7 hr.	0.4 hr.
η_{max}(20 km^3)	0.47 m	0.31 m	0.46 m	2.87 m
η_{max}(40 km^3)	0.96 m	0.62 m	0.87 m	5.83 m
η_{max}(80 km^3)	1.40 m	0.91 m	1.21 m	8.10 m
η_{max}(450 km^3)	4.84 m	3.24 m	3.10 m	19.04 m

Table 2: Maximum surface elevation computed off of several major cities for four CVV flank collapse volume scenarios, in 2' arc Atlantic grid.

Transatlantic propagation and far-field impact

After modeling the initial slide with THETIS for 5 min., and on the regional (500 m) grid with FUNWAVE for an additional 15 min., the leading wave train is sufficiently long to be accurately resolved on the coarser 2' Atlantic basin grid. The simulation of the transatlantic propagation with FUNWAVE shows that large waves, several meters high, would reach distant shorelines. Fig. 8 shows maximum elevation in the Atlantic ocean computed for the 80 km^3 case; clearly this tsunami would have damaging effects for cities along northwest Africa, western Europe, and eastern North America.

Table 2 summarizes maximum surface elevations computed offshore of different cities, for the four simulated CVV scenarios. Clearly, larger slide volumes result in larger waves in each location. Notably, for the largest slide scenario, the very large waves predicted by Ward and Day (2001) do not occur. However, waves simulated here would still pose a significant hazard to distant locations, such as the US east coast. A more detailed study of each location, however, using finer nested coastal grids, is necessary to predict actual inundation/runup and coastal impact.

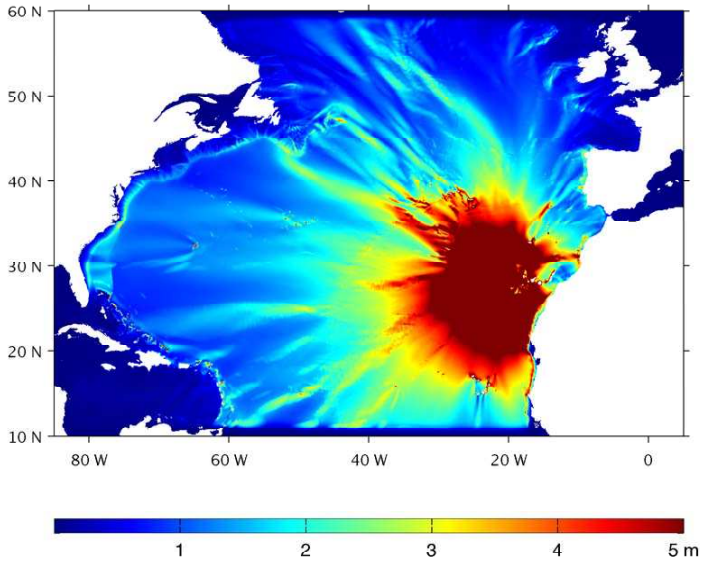

Fig. 8: Maximum surface elevation for the 80 km^3 CVV flank collapse case, computed with FUNWAVE in the 2' arc Atlantic grid.

To this effect, computations were performed, as a one-way coupling, in the four 30" coastal grids, with boundaries defined in Fig. 5. Maximum computed surface elevations are shown in Fig. 9 for the 80 km^3 case. These simulations were initialized: (i) for the N. North American grid, 6h after the initial slide; (ii) for the S. North American grid, 6h40' after the initial slide; (iii) for the European grid 1h20' after the initial slide; and (iv) for the African grid 20 min. after the initial slide. As could be expected from the proximity to La Palma, large waves occur along the northwest African coast. Even for this 80 km^3 case, waves are over 15 m offshore, near moderately large cities such as Dakhla, western Sahara. While in Europe, much of the tsunami energy is directed away from the continent (Fig. 8), there is substantial impact along the Portuguese coastline, particularly in Lisbon. Despite being far from the source, the US east coast is significantly impacted as well, although due to the tsunami directivity and wave guiding effects of nearshore bathymetry, some locations are impacted much more than others. Additionally, along the US east coast, maximum wave height decreases substantially as the tsunami propagates across the wide continental shelf. A higher-resolution grid than 30", however, would be necessary to determine whether this decrease is an accurate representation of the physics (e.g., wave breaking), or whether this is a result of insufficient resolution. This is left out for future work. In all cases, higher resolutions simulations would be necessary to accurately estimate the potential tsunami inundation.

CONCLUSIONS

Four scenarios of Cumbre Vieja Volcano (CVV) flank collapse were simulated, including the landslide tsunami generation, propagation, and near- and far-field impact. THETIS, a multi-fluid Navier-Stokes model with a VOF interface tracking, was used to calculate the free surface elevation generated by deforming slide motion. Wave trains were then input as initial conditions into FUNWAVE-TVD, a fully nonlinear Boussinesq model with extended dispersion properties, to study their propagation in the near field, around nearby islands. It is important to model dispersive effects in simulations, since landslide generated waves have relatively shorter wavelengths. Both of these numerical models have

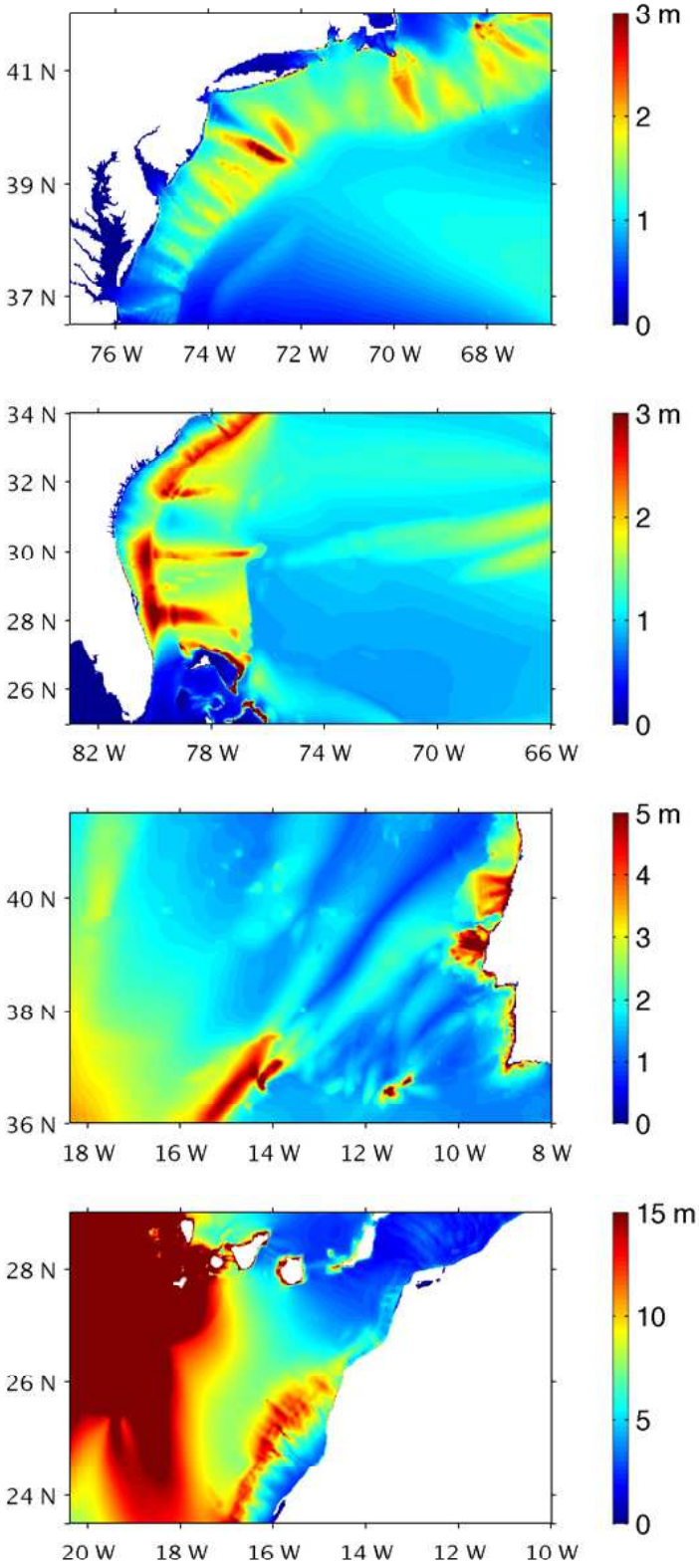

Fig. 9: Maximum surface elevation computed with FUNWAVE in 30" regional grids (Fig. 5, Table 1), for the 80 km^3 CVV case. From top to bottom: N. North Am.; S. North Am.; western Europe; western Africa.

been fully validated in other work, for landslide tsunami generation and propagation. While our overall findings are qualitatively consistent with those of Gisler et al. (2006) and Løvholt et al. (2008), waves computed in our study appear to be notably higher than in these earlier works and attenuation rates smaller. More details on the selection of slide scenarios, the modeling of 3D slides and related tsunami source generation with THETIS, and the analysis of these results around La Palma and in the near-field can be found in Abadie et al. (2012). The new computations with FUNWAVE presented here, of detailed near-field impact on the Canary islands and far-field impact in western Europe, northwest Africa, and eastern north America, in a series of nested grids, allows to quantify tsunami hazard as a function of the selected CVV scenario flank collapse.

ACKNOWLEDGEMENTS: Partial funding for this work was provided by grant #NA10NMS4670010 of the National Tsunami Hazards Mitigation Program (NTHMP), grant #EAR-09-11499 of the US National Science Foundation, and grant #037058 of the European Commission.

REFERENCES

Abadie, S., Caltagirone, J. P., and Watremez, P. (1998). Splash-up generation in a plunging breaker. *Comptes Rendus de l'Academie des Sci. Ser. IIB*, 326:553–559.

Abadie, S., Gandon, C., Grilli, S., Fabre, R., Riss, J., Tric, E., Morichon, D., and Glockner, S. (2008). 3D numerical simulations of waves generated by subaerial mass failures. Applicaiton to La Palma case. In *Proc. 31st Int. Coast. Eng. Conf.*.

Abadie, S., Harris, J., and Grilli, S. (2011). Numerical simulation of tsunami generation by the potential flank collapse of the Cumbre Vieja volcano. In *Proc. 21st Offshore Polar Eng. Conf.*.

Abadie, S., Harris, J., Grilli, S., and Fabre, R. (2012). Numerical modeling of tsunami waves generated by the flank collapse of the Cumbre Vieja Volcano (La Palma, Canary Islands) : tsunami source and near field effects. *J. Geophys. Res.*, (submitted):65 pps.

Abadie, S., Morichon, D., Grilli, S., and Glockner, S. (2010). Numerical simulation of waves generated by landslides using a multiple-fluid Navier-Stokes model. *Coast. Eng.*, 57:779–794.

Carracedo, J., Day, S., Guillo, H., and Gravestock, P. (1999). Later stage of volcanic evolution of La Palma, Canary Islands: rift evolution, giant landslides, and the genesis of the Caldera de Taburiente. *Geol. Soc. Am. Bull.*, 111:755–768.

Chen, Q. (2006). Fully nonlinear Boussinesq-type equations for waves and currents over porous beds. *J. Eng. Mech.*, 132:220–230.

Chen, Q., Kirby, J. T., Dalrymple, R. A., Kennedy, A. B., and Chawla, A. (2000). Boussinesq modeling of wave transformation, breaking, and runup. II: 2-D. *J. Waterw. Port, Coastal, Ocean Eng.*, 126:48–56.

Chen, Q., Kirby, J. T., Dalrymple, R. A., Shi, F., and Thornton, E. B. (2003). Boussinesq modeling of longshore currents. *J. Geophys. Res.*, 108:3362.

Cochonat, P., Lenat, J. F., Bachelery, P., Boivin, P., Corniglia, B., Deniel, C., Labazuy, P., Lipman, P., Oilier, G., Savoye, B., Vincent, P., and Voisset, M. (1990). Importance des dépôts gravitaires dans la mise en place d'un système vocano-sédimentaire sous–marin (Volcan de la Fournaise, Ile de la Réunion). *Comptes Rendus de l'Academie des Sci. Ser. IIB.*, 311:679–686.

Days, S. J., Watts, P., Grilli, S. T., and Kirby, J. T. (2005). Mechanical models of the 1975 Kalapana, Hawaii earthquake and tsunami. *Mar. Geol.*, 215:59–92.

Fabre, R., Riss, J., Tric, E., Lebourg, T., and Abadie, S. (2011). Potential collapse of the Cumbre Vieja volcanic ediface (La Palma Island,

Spain): numerical investigation of the failure model and potential volume. *Eng. Geol.*, (submitted).

Gisler, G., Weaver, R., and Gittings, M. (2006). SAGE calculations of the tsunami threat from La Palma. *Sci. Tsunami Hazards.*, 24:288–301.

Grilli, S. T., Baxter, C. D. P., Maretzki, S., Perignon, Y., and Gemme, D. (2006). Numerical simulation of tsunami hazard maps for the US East Coast. Report of Year 1 project. FMGlobal Project. Technical report, University of Rhode Island.

Grilli, S. T., Dubosq, S., Pophet, N., Perignon, Y., Kirby, J. T., and Shi, F. (2010). Numerical simulation and first-order hazard analysis of large co-seismic tsunamis generated in the Puerto Rico thrench: near-field impact on the North shore of Puerto Rico and far-filed impact on the US East Coast. *Nat. Hazards Earth Syst. Sci.*, 10:2109–2125.

Grilli, S. T., Ioualalen, M., Asavanant, J., Shi, F., Kirby, J., and Watts, P. (2007). Source constraints and model simulation of the December 26, 2004 Indian Ocean tsunami. *J. Waterw. Port, Coastal, Ocean Eng.*, 33:414–428.

Hirt, C. W. and Nichols, B. D. (1981). Volume of fluid (VOF) method for the dynamics of free boundaries. *J. Comput. Phys.*, 39:201–225.

Holcomb, R. T. and Searle, R. C. (1991). Large landslides from oceanic volcanoes. *Mar. Geotechnol.*, 10:19–32.

Inoue, K. (2000). Shimabara-Shigatusaku Earthquake and topographic changes by Shimabara Catastrophe in 1792. *Geogr. Reports Tokyo Metrop. Univ.*, 35:59–69.

Ioualalen, M., Asavanant, J., Kaewbanjak, N., Grilli, S. T., Kirby, J. T., and Watts, P. (2007). Modeling the 26th December 2004 Indian Ocean tsunami: Case study of impact in Thailand. *J. Geophys. Res.*, 112:C07024.

Karlsson, J. M., Skelton, A., Sanden, M., Ioualalen, M., Kaewbanjak, N., Pophet, N., Asavanant, J., and von Matern, A. (2009). Reconstructions of the coastal impact of the 2004 Indian Ocean tsunami in the Khao Lak area, Thailand. *J. Geophys. Res.*, 114:C10023.

Kennedy, A. B., Chen, Q., Kirby, J. T., and Dalrymple, R. A. (2000). Boussinesq modeling of wave transformation, breaking, and runup. I: 1D. *J. Waterw. Port, Coastal, Ocean Eng.*, 126:39–47.

Kirby, J. T. (2003). *Advances in Coastal Modeling*, chapter Boussinesq models and applications to nearshore wave propagation, surf zone processes and wave-induced currents, pages 1–41. Elsevier.

Kirby, J. T., Pophet, N., Shi, F., and Grilli, S. T. (2009). Basin scale tsunami propagation modeling using Boussinesq models: Parallel implementation in spherical coordinates. In *Proc. WCCE-ECCE-TCCE Jt. Conf. on Earthq. Tsunami.*, volume paper 100, page (published on CD).

Kirby, J. T., Shi, F., Harris, J. C., and Grilli, S. T. (2012). Sensitivity analysis of trans-oceanic tsunami propagation to dispersive and Coriolis effects. *Ocean Model.*, (submitted):42 pp.

Legros, F. (2002). The mobility of long-runout landslides. *Eng. Geol.*, 63:301–331.

Løvholt, F., Pedersen, G., and Gisler, G. (2008). Oceanic propagation of a potential tsunami from the La Palma Island. *J. Geophys. Res.*, 113:C09026.

Lubin, P., Vincent, S., Abadie, S., and Caltagirone, J. P. (2006). Three-dimensional large eddy simulation of air entrainment under plunging breaking waves. *Coast. Eng.*, 53:631–655.

Mader, C. L. (2001). Modeling the La Palma landslide tsunami. *Sci. Tsunami Hazards.*, 19:150–170.

Masson, D., Watts, A., Gee, M., Urgeles, R., Mitchell, N., Bas, T. L., and Canals, M. (2002). Slope failures on the flanks of the western Canary Islands. *Earth-Science Rev.*, 57:1–35.

Moore, J. G., Clague, D. A., Holcomb, R. T., Lipman, P. W., Normark, W. R., and Torresan, M. E. (1989). Prodigious submarine landslides on the Hawaiian Ridge. *J. Geophys. Res.*, 94:17465–17484.

Morichon, D. and Abadie, S. (2010). Vague générée par un glissement de terrain, influence de la forme initiale et de la loi de déformabilité du glissement. *La Houille Blanche.*, 1:111–117.

Oehler, J. F., Labazuy, P., and Lénat, J. F. (2004). Recurrence of major flank landslides during the last 2 Ma – history of Réunion Island. *Bull. Volcanol.*, 66:585–595.

Pararas-Carayannis, G. (2002). Evaluation of the threat of mega tsunamis generation from postulated massive slope failures of island stratovolcanoes on La Palma, Canary Islands, and on the island of Hawaii. *Sci. Tsunami Hazards.*, 20:251.

Pérignon, Y. (2006). Tsunami hazard modeling. Master's thesis, University of Rhode Island and Ecole Centrale de Nantes.

Robinson, J. E. and Eakins, B. W. (2006). Calculated volumes of individual shield volcanos at the young end of the Hawaiian Ridge. *J. Volcanol. Geotherm. Res.*, 151:309–317.

Ryan, W. B. F., Carbotte, S. M., Coplan, J. O., O'Hara, S., Melkonian, A., Arko, R., Weissel, A., Ferrini, V., Goodwillie, A., Nitsche, F., Bonczkowski, J., and Zemsky, R. (2009). Global Multi-Resolution Topography synthesis. *Geochem. Geophys. Geosystems.*, 10:Q03014.

Shi, F., Kirby, J. T., Harris, J. C., Geiman, J. D., and Grilli, S. T. (2012). A high-order adaptive time-stepping TVD solver for Boussinesq modeling of breaking waves and coastal inundation. *Ocean Model.*, 43-44:36–51.

Tappin, D. R., Watts, P., and Grilli, S. T. (2008). The Papua New Guinea tsunami of 1998: anatomy of a catastrophic event. *Nat. Hazards Earth Syst. Sci.*, 8:243–266.

Tehranirad, B., Shi, F., Kirby, J. T., Harris, J. C., and Grilli, S. T. (2011). Tsunami benchmark results for fully nonlinear Boussinesq wave model FUNWAVE-TVD, Version 1.0. Technical report, No. CACR-11-02, Center for Applied Coastal Research, University of Delaware.

Tinti, S., Manucci, A., Pagnoni, G., Armigliato, A., and Zaniboni, F. (2005). The 30th December 2002 landslide-induced tsunami in Stromboli: sequence of the events reconstructed from eyewitness accounts. *Nat. Hazards Earth Syst. Sci.*, 5:763–775.

Ward, S. N. and Day, S. (2001). Cumbre Vieja Volcano – potential collapse at La Palma, Canary Islands. *Geophys. Res. Lett.*, 28:397–400.

Watts, P., Grilli, S. T., Kirby, J. T., Fryer, G. J., and Tappin, D. R. (2003). Landslide tsunami case studies using a Boussinesq model and a fully nonlinear tsunami generation model. *Nat. Hazards Earth Syst. Sci.*, 3:391–402.

Wei, G., Kirby, J. T., Grilli, S. T., and Subramanya, R. (1995). A fully nonlinear Boussinesq model for free surface waves. Part I: Highly nonlinear unsteady waves. *J. Fluid Mech.*, 294:71–92.

Zhou, H., Moore, C. W., Wei, Y., and Titov, V. V. (2011). A nested-grid Boussinesq type approach to modelling dispersive propagation and runup of landslide generated tsunamis. *Nat. Hazards Earth Syst. Sci.*, 11:2677–2697.